Structures xxx (xxxx) xxx–xxx

Contents lists available at ScienceDirect

Structures

journal homepage: www.elsevier.com/locate/structures

Behaviour and design of composite steel and precast concrete transom for railway bridge application

O. Mirza[a,*], A. Talos[b], M. Hennessy[c], B. Kirkland[a]

[a] School of Computing, Engineering and Mathematics, Western Sydney University, Australia
[b] Graduate Engineer, CPB Contractors, Gate A11, Tallawong Road, Rouse Hill, NSW 2155, Australia
[c] Graduate Engineer, CPB Contractors, 177 Pacific Highway, North Sydney, NSW 2060, Australia

ARTICLE INFO

Keywords:
Railway bridges
Composite steel- concrete
Retrofitting

ABSTRACT

Currently most railway bridges in Australia require the frequent replacement of the timber transoms that reside in the railway system. Composite steel and precast reinforced concrete transoms have been proposed as the replacement for the current timber counterparts. This paper outlines the structural benefits of composite steel-concrete transoms for ballastless tracks when retrofitted to existing railway steel bridges. However, in existing studies, it is found that there is little investigation into the effect of derailment loading on reinforced concrete transoms. Therefore, this paper provides an investigation of derailment impact loading on precast reinforced concrete transoms. The paper herein investigates the derailment impact loading of a train through experimental testing and numerical analysis of conventional reinforced concrete transoms. The paper also evaluates the potential use of 3 different shear connectors; welded shear studs, Lindapter bolts and Ajax bolts. The results of the experimental tests and finite element models are used to determine whether each transom is a viable option for the replacement of the current timber transoms on the existing bridges in Australia and whether they provide a stronger and longer lasting solution to the current transom problem.

1. Introduction

Transoms are one of the most important components of a railway system. They are designed as load carrying elements of a railway bridge which span under the roadway and transfer the railway loads to the trusses and beams. Current timber transoms are the most commonly used however they are susceptible to biological and chemical degradation. This reduces their service life and requires frequent maintenance and replacement. In order to fulfill the current promotion of more sustainable material, alternative materials such as composite steel-concrete panels are starting to be implemented more. The reason being that composite steel-concrete provide a material which utilises the best attributes of each individual element providing higher strength, long service life and flexibility in design.

Transoms are rectangular members which rest on the ballast, laid perpendicular to the rails which they are fixed to by fastening systems. The term transom and sleeper refer to the same member and can be used interchangeably. The main purpose of transoms is to provide support to the track, by embedding itself into the substructure and preventing vertical, lateral and longitudinal movement [1]. Furthermore, according to the authors, these elements are vital in the transmission of applied axle loads on the superstructure to the substructures underlying ballast layer. Timber transoms were used in the early years of railroads due to their availability and suitability for the job. Over the past few decades, steel and concrete transoms have been adopted in modern railway tracks due to their favoured properties of durability and long service life [1]. These three materials have different advantages but no one material is more suitable for transom use. Existing research predominantly investigates the static and dynamic loading on railway bridge structures but are limited to derailment loading onto bridge structure itself and did not consider derailment impact loading scenarios for the transoms. Darwish [2] conducted a site investigation of a railway bridge in Baghdad. The author applied actual static live loading and dynamic loads to the bridge by passing a heavy locomotive over it at different speeds and stopping it in selective spots to understand how the structure reacts and deflects to different loading scenarios. Similar studies conducted by Griffin et al. [3,4] showed static tests on composite slabs, however, the studies did not investigate the derailment impact loading due to the locomotive.

To create a more consistent railway track in terms of quality and

* Corresponding author.
E-mail addresses: o.mirza@westernsydney.edu.au (O. Mirza), Andrew.Talos@nrtdd.com.au (A. Talos), Matt.Hennessy@cpbcon.com.au (M. Hennessy), b.kirkland@westernsydney.edu.au (B. Kirkland).

https://doi.org/10.1016/j.istruc.2019.03.006
Received 18 December 2018; Received in revised form 8 March 2019; Accepted 8 March 2019

comfort for the passengers, and to provide the long-term functionality required, an alternative material must be found. In the modern era, railway locomotive speeds have been increasing as detailed by González-Nicieza et al. [5] who state that improvements in transom design are mainly focused upon increasing the durability of the sleeper around the loading produced by higher speeds of the locomotive.

Impact loading is significant on railway bridges as it can have a significant effect on the design. Frýba & Pirner [6] conducted research which explained the static, dynamic and long term tests performed on bridges in the Slovak and Czech Republics but did not look into impact loading scenarios of these structures. Their static testing consists of measuring the vertical deflections of the greatest effect points, support settlements and squeeze of bearings while heavy vehicles applied the load on the railway bridges. The intention was to load the bridge with the heaviest static load possible, arranged to produce the greatest effects at the measured points.

Rebelo et al. [7] investigated the dynamic behaviour of a twin single span ballast railway viaduct structure. The authors studied the modal effects for the free vibration of the structure and the non-linear behaviour of the ballast while also analysing the free decay of the bridge, acceleration and ambient vibration as a result of a locomotive crossing the bridge. The authors explored ballasted type railway bridges in Austria but did not investigate ballastless tracks and their performance. Rebelo et al. [7] and Darwish [2] both research dynamic behaviour of ballast railway bridges but don't investigate ballastless tracks and how transoms in these systems react to derailment impact loading.

A full scale of field tests of a railway bridge in Los Angeles was conducted by Maragakis, Douglas & Chen [8] aiming to determine the seismic performance of a typical single span bridge, quantifying the beneficial effects the rails provide between the structure. Along with this the author also conducted a full-scale failure test of the deck-abutment connections determining the ultimate failure. The experimental studies conducted identified the ultimate strength reduced due to dynamic loading. In the case of the failure tests, the rails, ballast and ballast pan were removed from the west end of the bridge while the east end was left intact. The bridge was the loaded until failure at both ends and a comparison of the results was used to assess the role the ballast, ballast pan and track give in terms of the ultimate capacity of the abutment connections to the bridge. The need of derailment loading was ignored.

An experimental case study was conducted by Sorrenson & West [9] on a NSW steel railway bridge, in which stress, dynamic loading and acceleration responses were recorded under normal traffic loading conditions. A finite element structural sensitivity model was also constructed of the bridge using the experimental data and was used to determine variations in support and fixity conditions. Various passenger and freight train scenarios were constructed for the purpose of the model, which accurately represent realistic loading scenarios produced from passing trains involved in the field test. The bridge's dynamic structural responses were computed and compared to the experimental transient stress, acceleration, load and bending stresses obtained. From these tests, adjustments were made to the structural model to accurately correlate to the field test results. Looking over the research outlined in this study it is seen that the reaction of transoms due to derailment impact loading are not conducted, hence further studies are required in this field.

Hence, the purpose of this paper is to fill the knowledge gap of ballastless tracks under derailment loading scenarios in the plastic region. This paper also aims to determine the failure modes and strength of conventionally reinforced composite steel-concrete transoms in order to provide a guide for engineers to use in designing railway bridges.

2. Experimental study

Three conventionally reinforced specimens of 2100 mm length were tested. The cross-sectional area of the transoms is 600 mm wide x

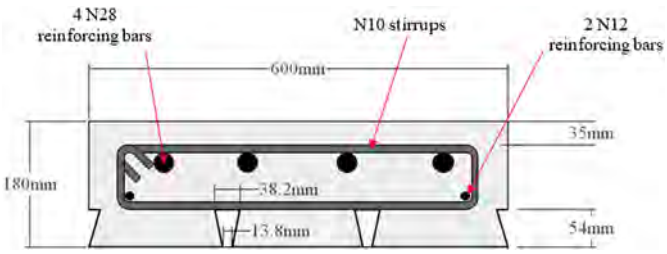

Fig. 1. Cross section dimensions.

180 mm thick. The transoms consist of N10 stirrups at 90 mm spacing, 2 N12 reinforcing bars of 2030 mm length and 4 N28 reinforcing bars of 2030 mm length. Figs. 1 and 2 show the details of cross section and longitudinal for the specimens, respectively. The types of connectors in the beams include 19 mm welded shear studs, 20 mm Ajax bolts and 29 mm Lindapter bolts as displayed respectively from left to right in Fig. 3.

Fig. 4 shows the location of the frame resisting the impact load and the location of the impact load on a longitudinal section view. The transom is set up underneath the impact loading machine, lined up with the drop hammer and bolted into place using a frame.

In order to simulate the derailment of a train, the frame should be able to withstand the reaction load of 600 kN. This value was found through initial analysis of Finite Element Modelling (FEM) of the composite steel and precast concrete transom. The derailment load was 180 kN static force which was applied to the transoms free end which in turn produced a reaction force of 110 kN on the frame. This static reaction was then increased by a factor of 4 which gives a 440 kN initial reading of what the reaction load should become. For conservative reasons as well as future proofing the frame, the reaction force that was adopted for the design was increased to 600 kN. From this, load design calculations were conducted and it was determined that 310UB46.2 members will be used for the main supporting sections and M24 10.9 bolts will be used to hold the frame together. A 200UB29.8 was use for the diagonal supporting member of the main members.

Fig. 5 illustrates the composite steel and precast transom and the sides of the frame were set up and bolted to the hardstand floor. The position of the transom was adjusted with a forklift until it was aligned 500 mm from the impact hammer from the edge as shown in Fig. 5. Fig. 6 demonstrates the displacement laser which was aligned with the impact point. Fig. 7 shows a rubber padding sheet was placed at the impact zone of the specimen to reduce the initial peak load experienced. The steel sections over the base of the transoms I-beam were bolted to the hard floor in order to prevent movement during the test as shown in Fig. 8.

3. Finite element model

3.1. Material properties

Through experimental analysis on the concrete presented in this research, Table 1 outlines the basic material properties.

Regarding the plastic behaviour of the concrete, there is limited research that investigates the type of procedure that should be adopted for explicit analysis of finite element modelling. However, two common techniques are the Drucker-Prager yield criterion and the Cap Plasticity model. Both techniques are applicable for use in the FEM software Abaqus where variables regarding the internal angle of friction, cohesion of the concrete and hardening of the cap are to be defined. The two methods are similar in nature being pressure-dependent and both incorporate the hardening of the material under high strain rates. Due to this high strain rate, the cap plasticity model will be incorporated into the modelling of the concrete. The use of this material modelling procedure is used in an investigation conducted by Remennikov and

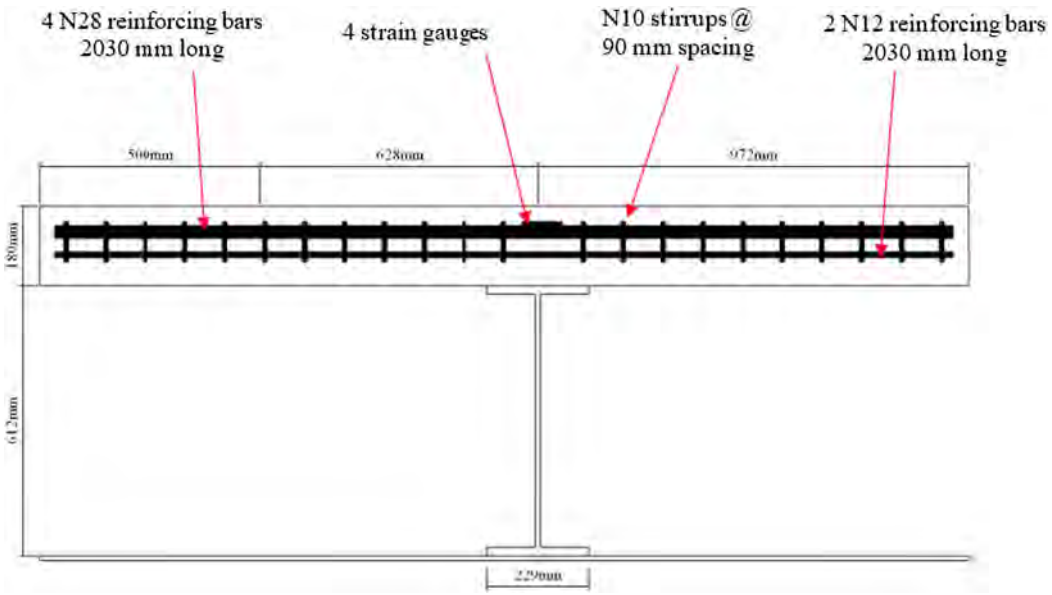

Fig. 2. Longitudinal section dimensions.

Fig. 3. Different types of shear studs for the specimens.

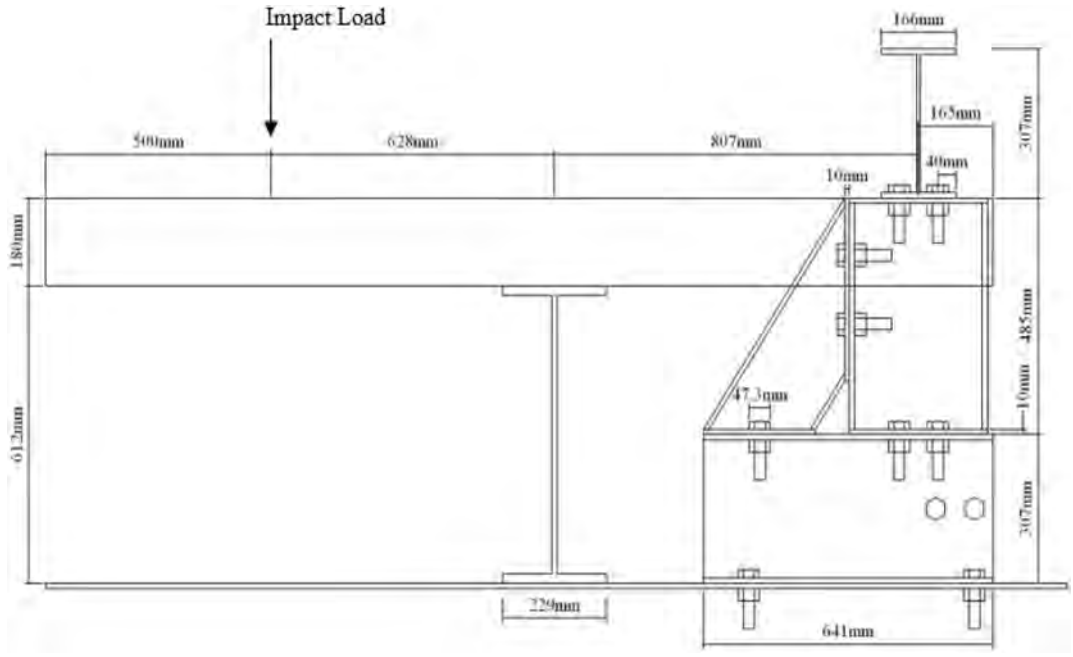

Fig. 4. Frame and impact loading locations.

Fig. 5. Experimental setup.

Fig. 6. Displacement laser.

Fig. 7. Rubber padding at impact zone.

Tahmeasebinia [10] where a similar loading scenario is used to produce the failure behaviour within a concrete slab. The properties are defined accordingly as presented in Table 2.

To complete the plasticity of concrete according to the Remennikov and Tahmeasebinia [10] model, the cap hardening also is required to be defined. The definition of this parameter is crucial to the accuracy of the results as they define how the concrete will react upon impact and how far the impactor will penetrate the concrete and hence, influencing the force produced in the transom. For this parameter, the values of stress and strain obtained from experimental analysis of the concrete

Fig. 8. Bolted I-beam.

Table 1
Elastic behaviour of concrete.

Property	Value
Compressive strength, f'_c	57 MPa
Young's modulus, E_c	34,652 MPa
Poisson's ratio, ν	0.2
Strain concrete, ε_c	0.003
Density, ρ	2400 kg/m^3

were obtained and inserted into the required fields for the cap hardening sub option.

Lastly, exclusive to explicit analysis, the density of concrete must also be defined to accurately model the propagation of the stress wave through the structure. The value of density was taken as 2400 kg/m^3 which is a general value for this parameter. This value was taken due to information regarding the density of the experimental specimens not being recorded. The initial material properties for the steel elements within the Abaqus model are presented in Table 3 where the ratios for determining ultimate stress (σ_{us}), plastic strain (ε_{ps}), and ultimate strain (ε_{us}) are summarised by [3]. The elastic modulus, E for all steel was taken as 200 GPa. There is low yield capacity in the support beam with a yield strength of 300 MPa as displayed in Table 3. This is because the steel beam that is currently used on the Sydney Harbour Bridge was designed in the 1930s. Therefore, the same capacity must also be used in this analysis to accurately simulate the behaviour of the transom.

For explicit analysis, the density of each material is also required to be defined so the finite element software can accurately calculate the propagation of the stress wave through the structure. The density of all steel elements was taken as 7850 kg/m^3.

3.2. Element type and mesh

The elements used for the nodes in this investigation are the C3D8R element. As stated by Mirza [11,12], this is derived from the five aspects of their behaviour; the family, degrees of freedom, number of nodes, formulation and integration. The C3D8R element is used for all parts except for the conventional reinforcement where the truss element, T3D2 is used as shown in Table 4.

Meshing is a crucial aspect of the finite element model. Due to the nature of the loading, the model is run under explicit analysis. Hence, the simulation time is directly proportionate to the smallest element length within the model. The increment size is calculated based upon the length of time taken for a wave propagating at the speed of sound to

Table 2
Cap plasticity concrete material.

Cohesion (MPa)	Internal angle of friction (β)	Cap eccentricity parameter (R)	Initial cap yield surface position	Ratio of flow stress (K)
4.70567	51°	0.65	1.1×10^{-3}	1

Table 3
Steel material properties.

Element	Yield stress (MPa)	σ_{us} (MPa)	ε_{ps}	ε_{us}
Support beam	300	1.28 σ_{ys}	10 ε_{ys}	30 ε_{ys}
Stiffener	300	1.28 σ_{ys}	10 ε_{ys}	30 ε_{ys}
Reinforcing steel	500	1.28 σ_{ys}	9 ε_{ys}	40 ε_{ys}
Prestressing steel	500	1.28 σ_{ys}	9 ε_{ys}	40 ε_{ys}
Bondek II	550	N/A	20 ε_{ys}	N/A
Shear studs	420	N/A	25 ε_{ys}	N/A

Table 4
Element types used in the FE model.

Part	Element type
Concrete	C3D8R
Bondek II	C3D8R
Shear studs	C3D8R
Loading plate	C3D8R
Support beam	C3D8R
Conventional reinforcement	T3DR

travel across the smallest length. Therefore, to reduce computation times, mesh sizing was kept large. Explicit analysis operates based upon the propagation of the deformation wave which is limited to the speed of the sound barrier. To calculate the increment size during analysis, it is therefore based upon the length of the smallest element and the amount of time taken for a propagated deformation wave travelling at the speed of sound to travel across the element. Hence, it is concluded that the mesh sizing used in the model is directly proportional to the simulation time taken to run explicit analysis. The optimisation of the mesh was performed with consideration to the accuracy of the results produced and the computational time required.

Due to the large amount of parts and interactions, mesh sizes were kept on the larger side to reduce simulation times and possibility of the stress wave exceeding the sound barrier and causing errors. The mesh sizing used during the modelling procedure is outlined in Table 5.

3.3. Contact interactions

The importance of contact interaction is greatly increased when the composite structure is considered since the load-bearing capacity of the structure is dependent upon the interaction between one or more elements. Again, to reduce simulation times, tie constraints were used for all surfaces except for the contact between the impactor and the concrete. Table 6 illustrates the interactions used for the finite element analysis herein.

Due to the complexity of each model and the amount of time taken to run each numerical analysis, the interactions were kept simple with the use of tie constraints. However, the use of tie constraints between the shear studs and concrete, which is the area of the most complexity in regard to interaction, can be assumed to be appropriate since the shear stud has fully bonded with the high-strength grout that was used during the fabrication of the transom for experimental analysis. Furthermore, a surface-based tie constraint was purposely chosen in this scenario to make the translational and rotational motion as well as all other active degrees of freedom equal for a pair of surfaces. This is mainly due to the impacts loading that were subjected to the transom. Additionally, the tie constraint is also deemed appropriate when considering welded connections such as the stiffener to the support beam and the welded headed shear stud to the support beam. Fig. 9 illustrates the interactions between the Bondek II sheeting, shear studs, stiffener and concrete.

Table 5
Mesh sizing used for explicit analysis.

Part	Mesh size
Concrete	60
Support beam	75
Shear studs	20
Stiffener	75
Bondek II	75

3.4. Loading conditions

To compare the results obtained in this numerical analysis with the experimental analysis conducted, the target height above the transom was required to be 2 m. Initially the impactor was displaced to the 2 m target height and relied upon the gravity loading as defined previously to produce the velocity required for the impact. However, this caused an unnecessary and significant increase in simulation times. Therefore, the impactor was placed 200 mm above the surface of the transom and subjected to the velocity produced from a 2 metre drop using a predefined field, calculated to be 6.264 m/s as shown in Fig. 10. For the impact loading in the finite element model, an impactor of 100 mm diameter is used to replicate the experimental conditions the transoms will be subjected to. For the experimental studies, the impactor that is used has a weight of 595 kg and is made from steel. Hence, the impactor must also be modelled in Abaqus. This paper does not aim to produce the behaviour of the impactor itself; hence, the material was of basic attributes and was modelled as a rigid element to reduce simulation times. The placement of the impactor is displayed in Fig. 10.

3.5. Boundary conditions

To replicate the experimental setup, Fig. 11 shows the boundary conditions used in the finite element model. To resist the reaction force produced by the impact loading, BC-1 is placed 165 mm before the end of the beam and resists displacements in the y and z-directions. For the bolting of the support beam to the ground, BC-2 is placed on the bottom face of the flange of the beam and resists displacement only in the z-direction. Finally, BC-3 is placed on the impactor to resist displacements in the x and z directions to only allow movement in the y-direction. During experimental analysis, the impact slid vertically on set of rails. Therefore, movements in the x and z-directions are required to be controlled.

4. Results and discussion

4.1. Conventionally reinforced transom with welded shear studs (CRW)

To analyse the behaviour of the concrete, there are three main points during the impact that has been outlined and discussed. These are represented by Points A, B and C in Fig. 12 where the peak deflection during loading, initial permanent deformation after the initial contact and the final permanent deformation is highlighted by these points respectively. Point A in Fig. 12 is 31 mm as a result from the first

Table 6
Interactions between elements.

Interface	Interface type	Master surface	Slave surface
Bondek on the support beam	Tie constraint	Support beam	Bondek II
Bondek on the concrete	Tie constraint	Bondek II	Concrete
Shear stud inside concrete	Tie constraint	Shear stud	Concrete
Shear stud on support beam	Tie constraint	Shear stud	Support beam
Stiffener welded to support beam	Tie constraint	Stiffener	Support beam
Impactor on the concrete	General contact (explicit)	Impactor	Concrete
Conventional reinforcement inside concrete	Embedded constraints	Conventional reinforcement	Concrete

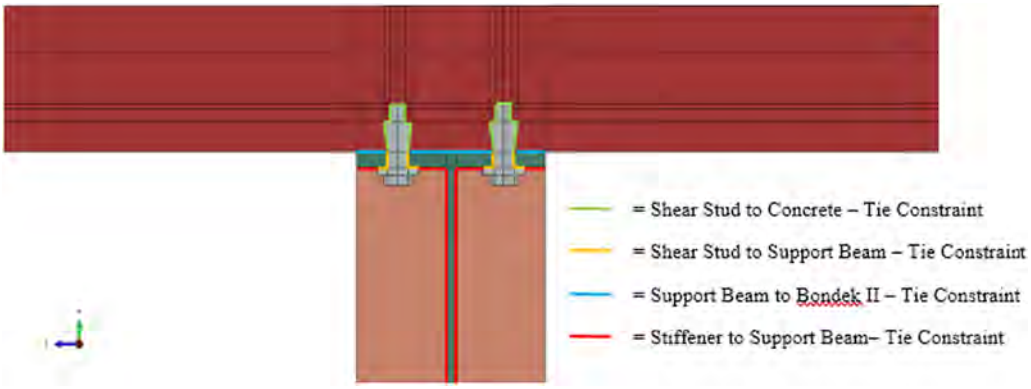

Fig. 9. Interactions between elements.

contact between the impactor and the concrete. The peak displacement produced is 47 mm. Following the initial impact, the concrete returns to a displacement of 19 mm shown in Point B. This corresponds to a displacement of 16 mm for the experimental data at the same point in loading and a discrepancy of 3 mm, corresponding to an 18% discrepancy between the two sets of data. The final permanent deformation at Point C in the simulation is shown to be 18 mm. The experimental data displays a similar permanent deformation of approximately 14 mm when averaged, corresponding to a discrepancy of 4 mm and 24% decrease in deflection. During experimental testing, the specimen was first subjected to an impact loading at a 1 metre height since it was the first specimen to be tested and was treated as a trial.

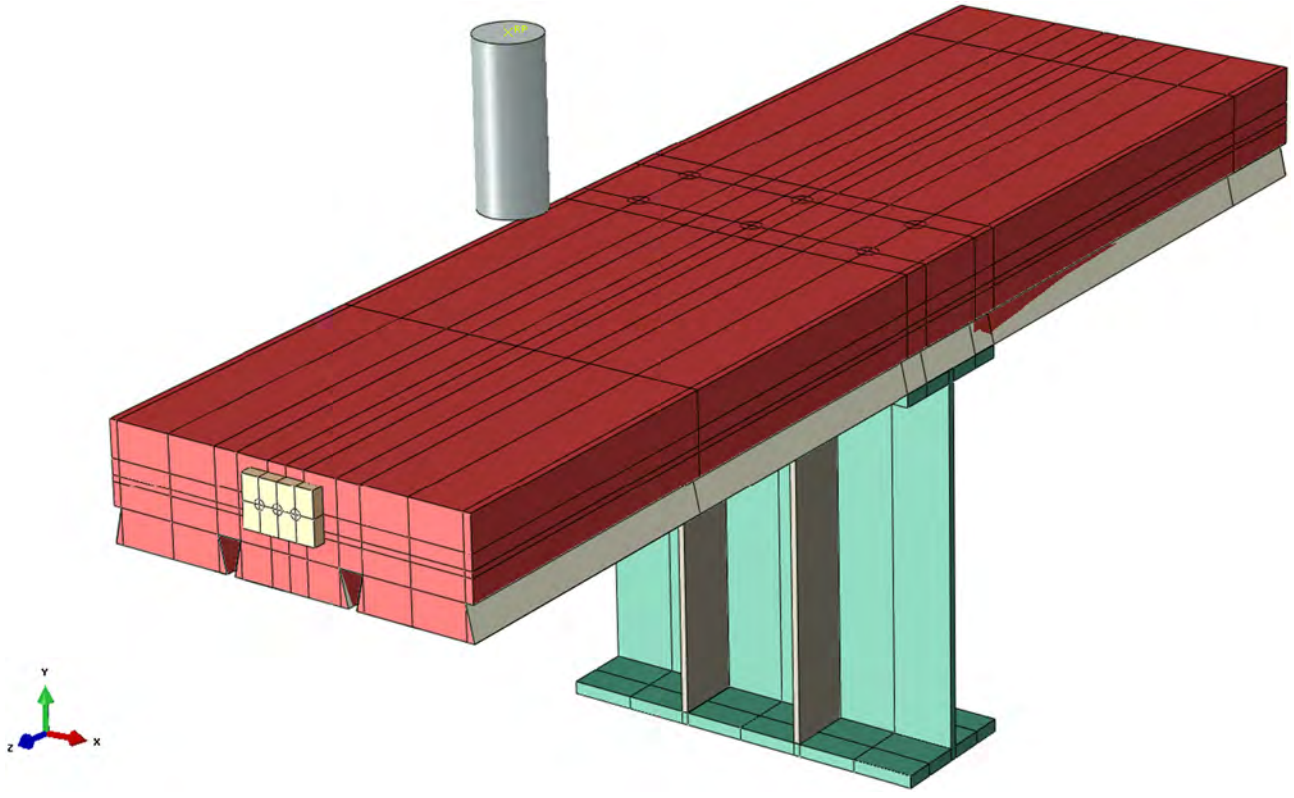

Fig. 10. Impactor load.

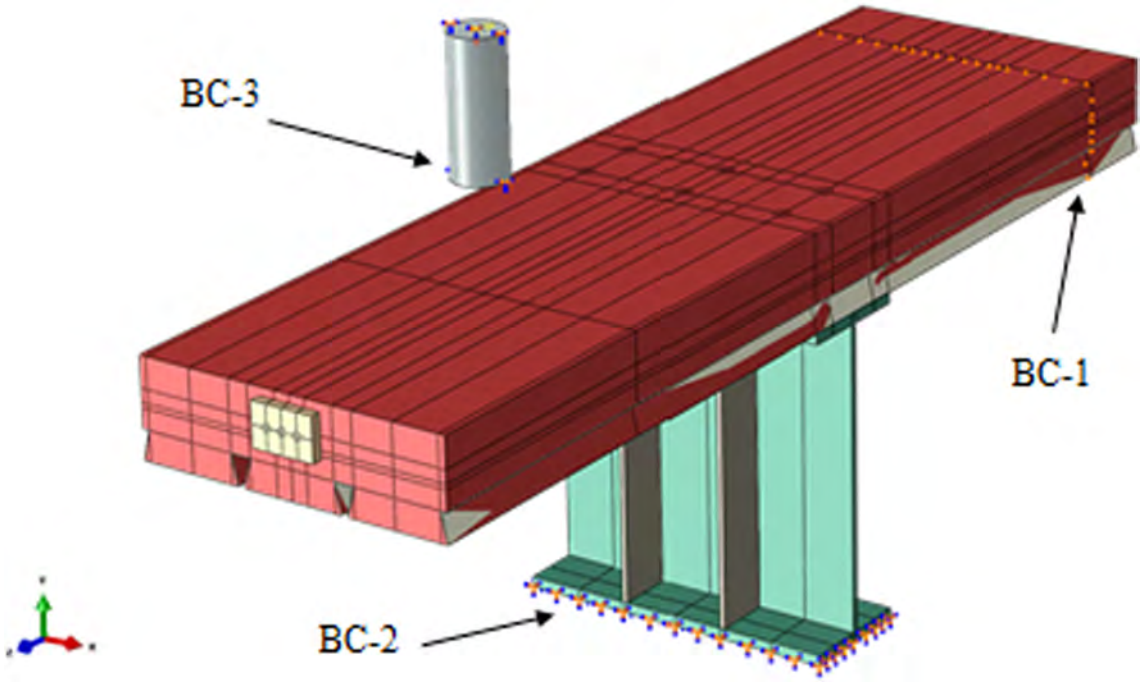

Fig. 11. Impactor load.

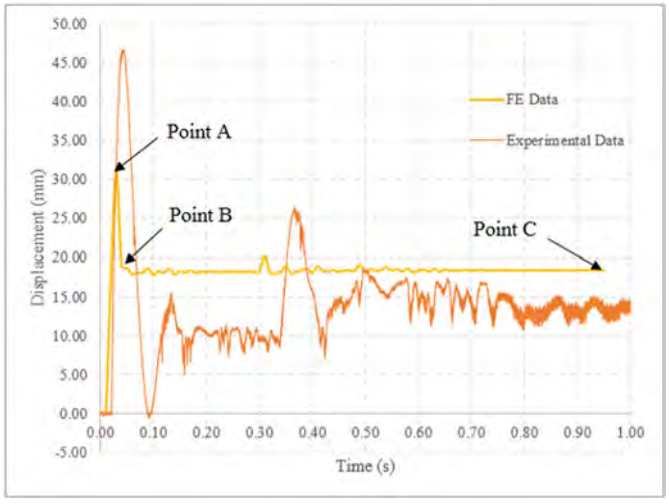

Fig. 12. Deflection behaviour for CRW.

However, the specimen was damaged prior to the 2 m impact test and this significantly influences the response of the concrete to the next impact, hence, large discrepancies between the results for numerical and experimental analysis are produced.

Region (1) in Fig. 13a and b outline the cracking through the connection that occurs in both the specimen and model where the stress has reached 10 MPa. The region highlighted here is also subjected to large amounts of bending and hence, excessive cracking occurs. Region (2) displays the stress occurring around the impact zone. Similarly, with the previous regions, excessive cracking propagates from this area due to the large strain produced on the surface of the concrete during the impact loading. For the side of the concrete, Region (3) highlights the similarities in stress propagation between the results for numerical and experimental analysis in Fig. 14a and b. Due to the previous loading, the concretes response to the loading is significantly changed for the next loading and as Fig. 14a displays, severe cracking has propagated from the impact zone and transferred to the Bondek II profile sheeting and has caused delamination.

4.2. Conventionally reinforced transom with AJAX bolts (CRA)

From Fig. 15, Point A displays the displacement of the impact zone for the corresponding the maximum peak load the panel can withstand and is estimated to be 28 mm. The peak displacement produced by the experimental data is 42 mm, corresponding to a difference of 14 mm. However, since this displacement is large when compared to the remaining data for the finite element model and occurs for a small amount of time, this result can be considered negligible.

After the first contact, the impactor is separated from the concrete and the transom shows signs of permanent deformation as the concrete returns to a displacement of 14 mm outlined by Point B. This corresponds to a displacement of 17 mm for the experimental data at the same point in loading and a discrepancy of 3 mm, corresponding to a 21% discrepancy due to the large vibration experienced by the beam after the initial impact. The permanent deformation at Point C in the simulation is shown to be 15 mm. The experimental data displays a similar permanent deformation of 16 mm, corresponding to a discrepancy of 1 mm and 7% increase in deflection.

Fig. 16a and b displays the cracking on the top of the experimental specimen and FE model respectively through means of stress contour plotting. Regions (1) and (2) outline the cracking through the connection that occurs in both the specimen and model where the stress has reached 10 MPa. The region highlighted here is also subjected to large amounts of bending and hence, excessive cracking that occurred. Region (3) displays the stress occurring around the impact zone. Similarly with the previous regions, excessive cracking propagates from this area due to the large strain produced on the surface of the concrete during the impact loading.

For the side of the concrete, Regions (1) and (2) again highlight the similarities in stress propagation between the results for numerical and experimental analysis in Fig. 17a and b. From the bending of the concrete, there is a large compressive force created around the connection as a consequence of the stiffness created in the concrete by the connection to the support beam. Region (1) displays the increased stress in the FE model occurring in this region and therefore, the cracking that would occur. Fig. 17a confirms this assumption with the excessive failure and crushing occurring in the concrete being outlined in Region

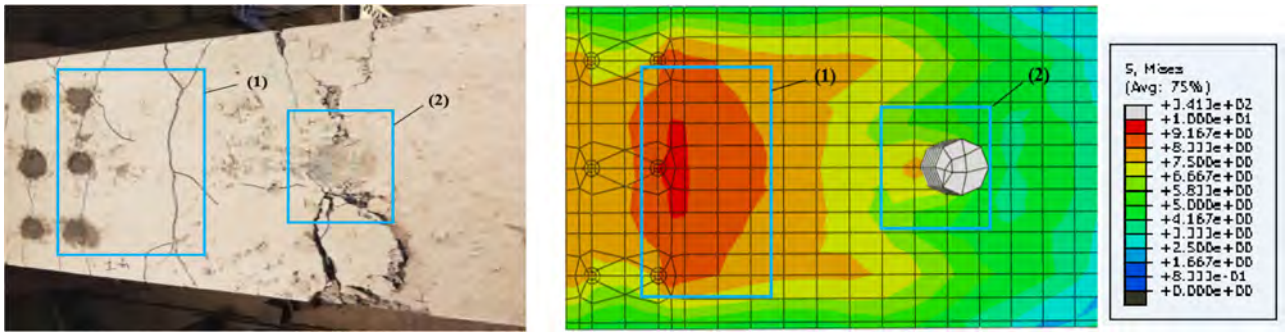

a: Cracking behavior for CRW

b: Stress distribution for CRW

Fig. 13. a: Cracking behaviour for CRW
b: Stress distribution for CRW.

(1). Region (2) displays the transfer of stress from the concrete to the Bondek II profile sheeting. The numerical results illustrate the stress propagating towards the sheeting and are validated by the experimental results displaying the same propagation.

4.3. Conventionally reinforced transom with Lindapter bolts (CRL)

Point A in Fig. 18 is 29 mm as a result from the first contact between the impactor and the concrete. Comparatively, the peak displacement produced by the experimental data is 37 mm, corresponding to a difference of 8 mm. After the first contact, the transom shows signs of permanent deformation as the concrete returns to a displacement of 10 mm outlined by Point B. This corresponds to a displacement of 13 mm for the experimental data at the same point in loading and a discrepancy of 4 mm, corresponding to a 42% discrepancy between the two sets of data. The final permanent deformation at Point C in the simulation is shown to be 12 mm. The experimental data displays a similar permanent deformation of approximately 11 mm when averaged, corresponding to a discrepancy of 1 mm and 5% decrease in deflection.

Region (1) in Fig. 19a and b outline the cracking through the connection that occurs in both the specimen and model where the stress has reached 10 MPa. The region highlighted here is also subjected to large amounts of bending and hence, excessive cracking occurred. Due to the stiffness added by the shear studs, bending also happens in the area outlined by Region (2) and cracking occurs in both the numerical and experimental results. Lastly, Region (3) displays the stress occurring around the impact zone. Similarly, with the previous regions, excessive cracking propagates from this area due to the large strain produced on

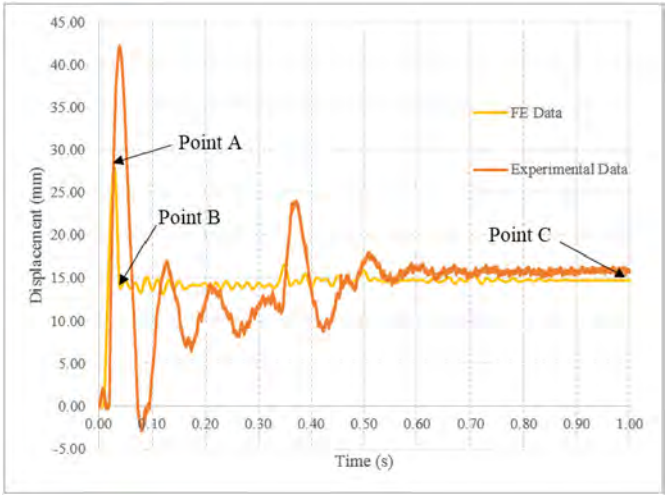

Fig. 15. Deflection behaviour for CRA.

the surface of the concrete during the impact loading.

For the side of the concrete, Region (1) again highlights the similarities in stress propagation between the results for numerical and experimental analysis in Fig. 20a and b. The stress propagating from the top surface of the concrete in the FE model is approximately 5–6 MPa which as stated previously, will cause initial cracking but not severe. However, a significant difference between the two images is the severe cracking occurring in the bottom left of Region (1) of Fig. 15a.

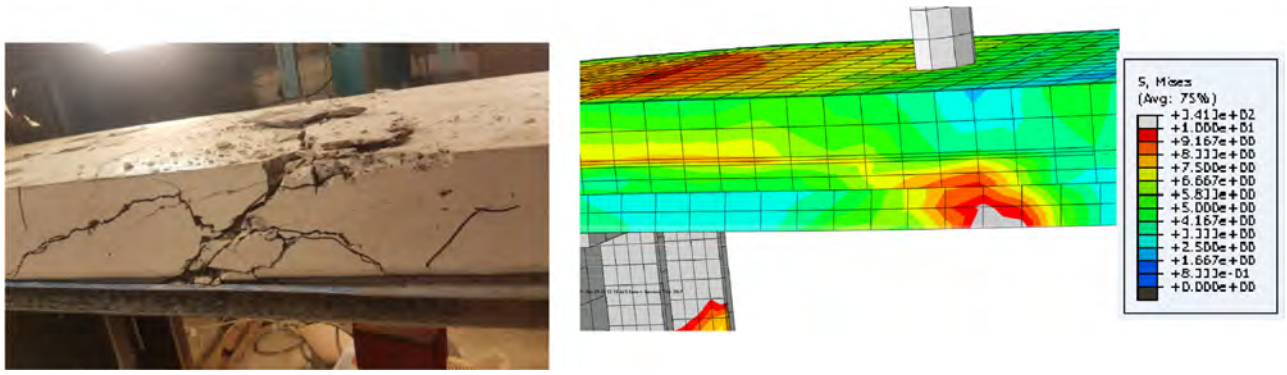

a: Cracking behavior for CRW

b: Stress distribution for CRW

Fig. 14. a: Cracking behaviour for CRW
b: Stress distribution for CRW.

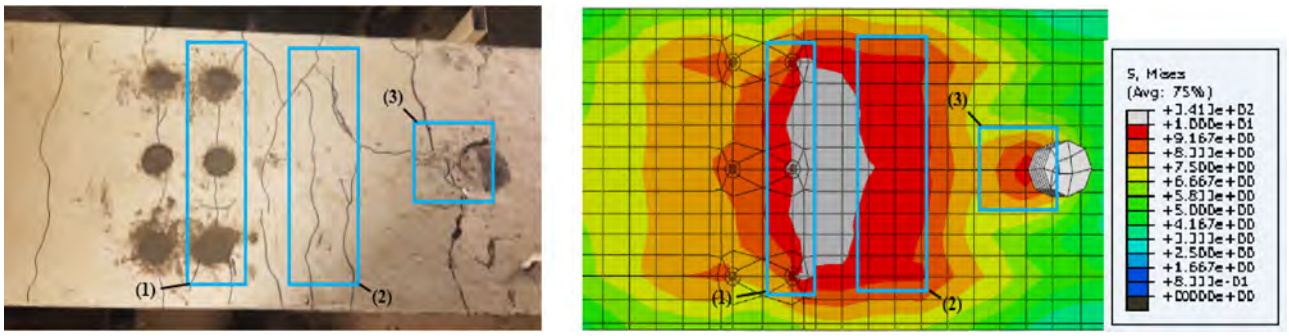

a: Cracking behavior for CRA

b: Stress distribution for CRA

Fig. 16. a: Cracking behaviour for CRA
b: Stress distribution for CRA.

4.4. Comparative study

General observations showed that all tests experienced shear failures in the concrete around the impact zone region. All the tests showed minimal cracking on the sides towards the supports with more significant cracks on the top face through the grouting. All the tests showed concrete crushing at the impact zone as a result of the repeated dynamic impact loading phenomenon between the drop hammer and the transom. It was also observed that all of the cross sections at the loaded end had delamination of the Bondek sheeting from the concrete transom.

For this comparative section, the data that is being compared is the real load experienced, which was found from Point B on the graphs and the permanent damage deformation of the transom. The reason for the comparison of this data is because they are part of the critical information required for determining which shear stud provides the strongest and most reliable connection for the transom.

For the comparison of the results for the conventionally reinforced specimens, both the CRA and CRL will be compared to the CRW as they are the most commonly used shear connection in industrial practice. At Point B, it can be observed that the welded shear stud has a slightly higher load capacity in comparison to the bolted connections even though the transom for the WSBC was impacted loaded from a 1 m height previously. The real load for CRW was found to be 454.2 kN while the CRL and CRA bolts showed a decrease in the real load of 4.9% and 10.2% respectively. This is due to the CRW having a larger surface area on the head that is situated in the concrete allowing for the load to be distributed better as shown in Fig. 21. The tie and strut effect of the CRL means it is over a certain tensile resulting in lower load capacities

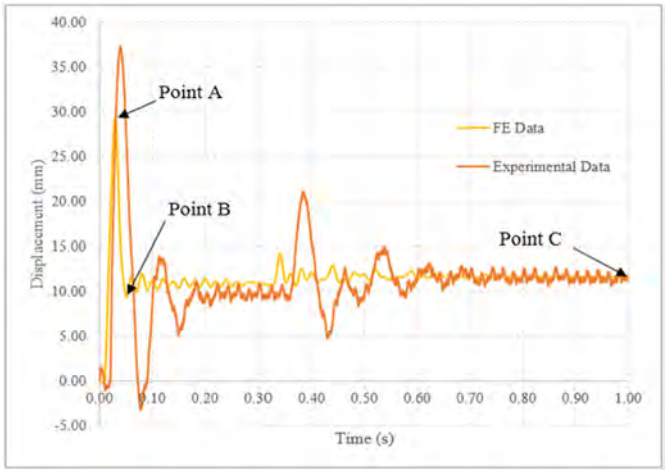

Fig. 18. Deflection behaviour for CRL.

due to premature concrete failure. The permanent damage deformation of the CRL showed a 1.5 mm difference corresponding to an 11.3% decrease in comparison to the CRW, whereas the CRA bolts showed a displacement increase of 2.6 mm, corresponding to an overall permanent damage deformation increase of 19.5%. Fig. 22 shows the comparison of the displacement versus time for the conventionally reinforced specimens. For the conventional reinforcement results for both load and permanent damage deformation it was found that the highest discrepancy was 19.5%. Since this is a relatively small variance this

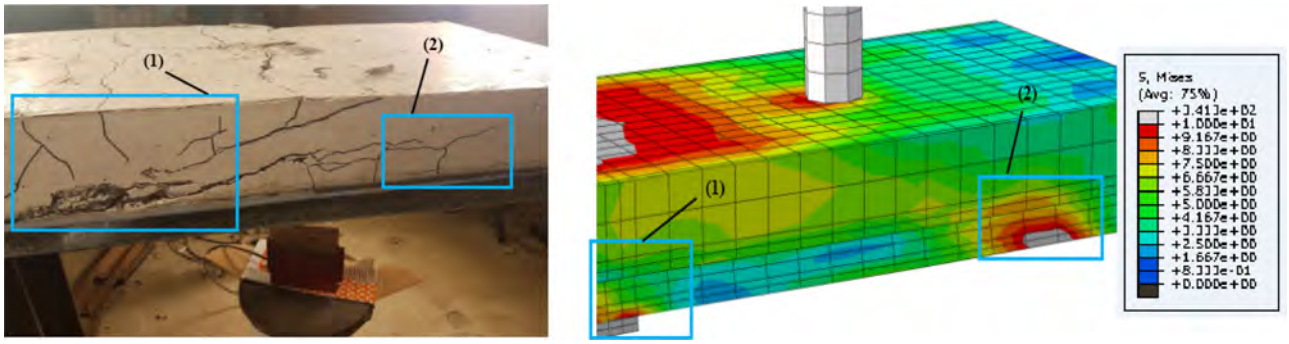

a: Cracking behavior for Experimental CRA

b: Stress distribution for CRA

Fig. 17. a: Cracking behaviour for Experimental CRA
b: Stress distribution for CRA.

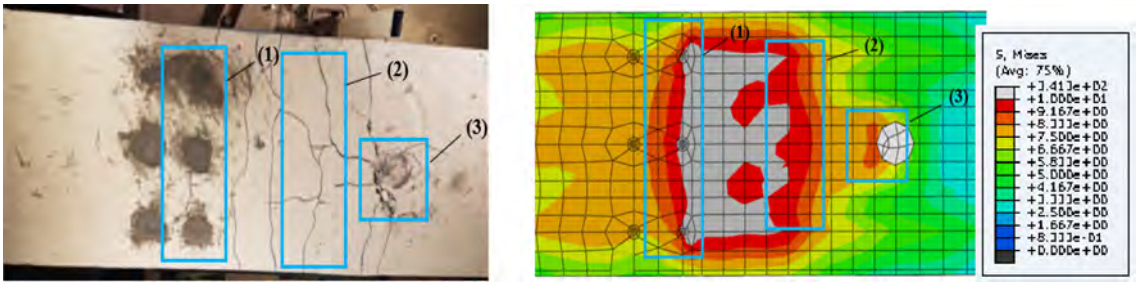

a: Cracking behavior for CRL b: Stress distribution for CRL

Fig. 19. a: Cracking behaviour for CRL
b: Stress distribution for CRL.

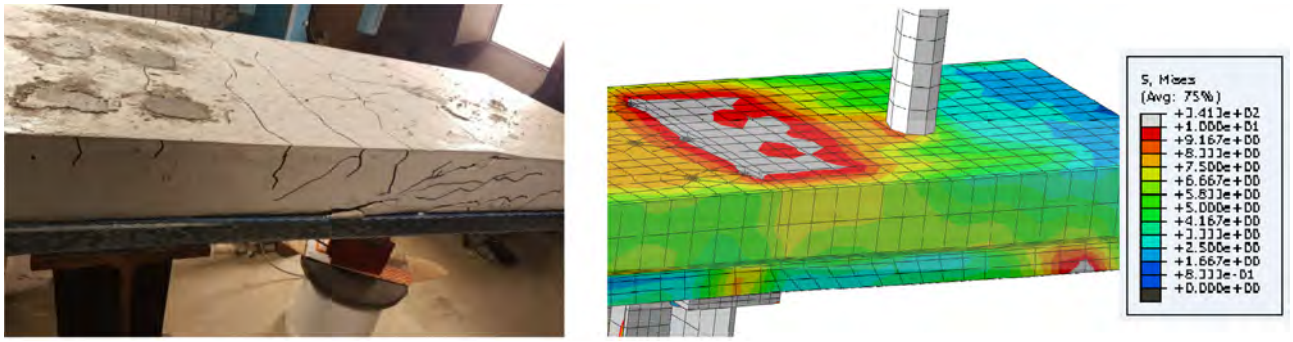

a: Cracking behavior for Experimental CRL b: Stress distribution for CRL

Fig. 20. a: Cracking behaviour for Experimental CRL
b: Stress distribution for CRL.

discrepancy could be due to manufacturing/fabrication stage errors or due to the differences in vibrations near the shear studs. From the results discussed above it appears that more tests need to be conducted in order to gain a higher confidence in the results.

5. Conclusions

Three transoms were experimentally tested and modelled to determine the detailed failure behaviour of the transom and the feasibility in replacing the current timber transoms that reside on the existing steel railway bridge network. The transoms were varied using three different types of shear connectors: AJAX bolts, welded headed shear studs and Lindapter bolts to analyse the change in strength given by these shear connectors.

The following conclusions were obtained from the research presented herein:

1. No signs of significant failure within the concrete transom or existing steel structure were observed for either the experimental or numerical analysis.
2. Initial and severe cracking was produced particularly around the connection due to the bending moment produced upon impact. However, the capacities of the reinforced concrete transoms exceeded the intended design load and have resulted in an overly conservative design.
3. The type of shear connector was observed to have a significant effect within the conventionally reinforced transoms. Similar trends in deformation were displayed in all connectors. However, the Lindapter bolt displayed the lowest peak and residual deflections due to the extra surface area bonding to the concrete and larger diameter, providing more stiffness to the concrete.
4. Discrepancies between the numerical and experimental were minimal, promoting the validity and future use of these finite element models for parametric studies and investigations into further detail of the failure behaviour.

Current researchers mainly investigate the performance of members under static loading scenarios, hence why this paper herein has been

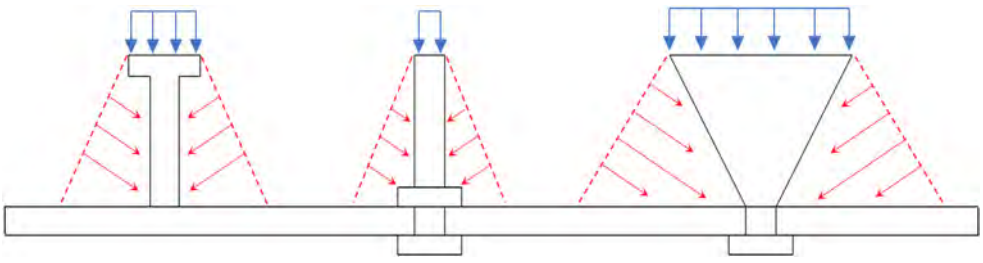

Fig. 21. Load and stress distribution on the shear connectors used (Left: Welded shear stud, Middle: Ajax bolt, Right: Lindapter bolt).

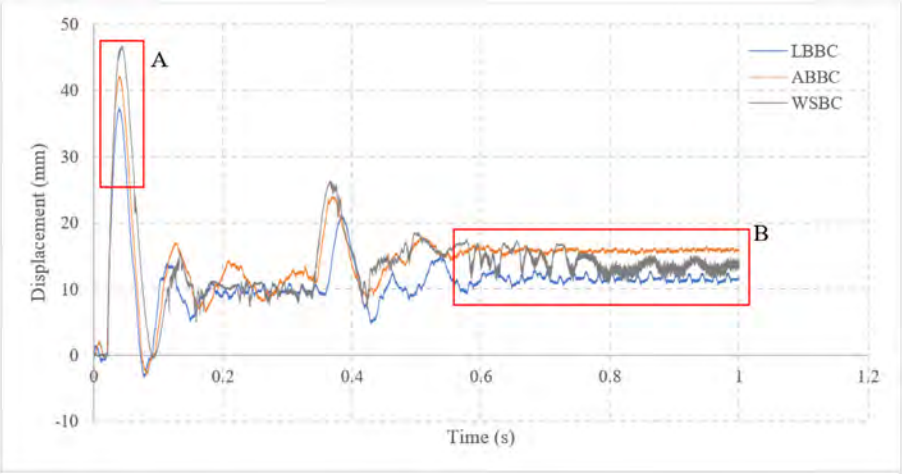

Fig. 22. Displacement versus time comparison for conventionally reinforced specimens.

developed to fill the knowledge gap of ballastless tracks under derailment loading scenarios in the plastic region. This paper determines the failure modes and ultimate capacity of the specimens which will later be used in order to provide a guideline for engineers to use in designing railway bridges under derailment impact loading.

Acknowledgements

The authors would like to thank Mr. Zac White from Western Sydney University and the University of Wollongong's technical staff for their help during the testing stage. We would also like to thank the industry partners Transport for New South Wales for sharing their technical knowledge and EJF Engineering for manufacturing the frame.

References

[1] Remennikov A, Kaewunruen S. A review of loading conditions for railway track structures due to train and track vertical interaction. Struct Control Health Monit 2008;15(2):207–34.
[2] Darwish AM. Static and dynamic loading test of a railway bridge. Acta Technica Corviniensis - Bulletin of Engineering 2015;8(2):145–8.
[3] Griffin D, Mirza O, Kwok K, Kaewunruen S. Composite slabs for railway construction and maintenance: a mechanistic review. The IES Journal Part A: Civil & Structural Engineering 2014;7(4):243–62.
[4] Griffin D, Mirza O, Kwok K, Kaewunruen S. Finite element modelling of modular precast composites for railway track support structure: a battle to save Sydney Harbour Bridge. Aust J Struct Eng 2015;16(2):150–68.
[5] González-Nicieza C, Álvarez-Fernández MI, Menéndez-Díaz A, Álvarez-Vigil AE, Ariznavarreta-Fernández F. Failure analysis of concrete sleepers in heavy haul railway tracks. Eng Fail Anal 2008;15(1–2):90–117.
[6] Frýba L, Pirner M. Load tests and modal analysis of bridges. Eng Struct 2001;23(1):102–9.
[7] Rebelo C, Simões da Silva L, Rigueiro C, Pircher M. Dynamic behaviour of twin single-span ballasted railway viaducts - field measurements and modal identification. Eng Struct 2008;30(9):2460–9.
[8] Maragakis E, Douglas BM, Chen Q. Full-scale field tests of a railway bridge. Railway Age 1995;196(9):101–3.
[9] Sorrenson PJ, West MP. "Field test validation of a railway bridge model by structural dynamic sensitivity analysis", paper presented to conference on railway engineering, Wollongong, 10-13. Nov 2002;2002.
[10] Remennikov A, Tahmeasebinia F. Simulation of the reinforced concrete slabs under impact loading. Australasian Structural Engineering Conference (ASEC), June 2008;2008:26–7.
[11] Mirza O and Uy B, (2010), "Effect of combination of axial tensile and shear loading on the behaviour of headed stud steel anchors.", J Eng Struct, An International Journal, v 32, pp. 93–105.
[12] Mirza O, Kaewunruen S. "Influence of shear bolt connections on modular precast steel-concrete composites for track support structures", Steel and. Compos Struct 2018;27(5):647–59.